Mon. Not. R. Astron. Soc. **381,** 1287–1300 (2007) doi:10.1111/j.1365-2966.2007.12332.x

Warp diffusion in accretion discs: a numerical investigation

Giuseppe Lodato[1,2]★ and J. E. Pringle[1,2]

[1]*Department of Physics and Astronomy, University of Leicester, Leicester LE1 7RH*
[2]*Institute of Astronomy, Madingley Road, Cambridge CB3 0HA*

Accepted 2007 August 8. Received 2007 August 8; in original form 2007 February 1

ABSTRACT

In this paper we explore numerically the evolution of a warped accretion disc. While previous analyses have concentrated on the case where the disc is thick enough that the warp propagates as a wave, we focus here on the opposite regime of a thin disc, where the warp evolves diffusively. By comparing the numerical results to a simple diffusion model, we are able to determine the diffusion coefficient of the warp, α_2, as a function of the relevant disc parameters, such as its thickness and especially its viscosity. We find that while in general the disc behaviour is well reproduced by the diffusion model and for relatively large viscosities the warp diffusion is well described by the linear theory (in particular confirming that the warp diffusion coefficient is inversely proportional to viscosity), significant non-linear effects are present as the viscosity becomes smaller, but still dominates over wave-propagation effects. In particular, we find that the inverse dependence of the diffusion coefficient on viscosity breaks down at low viscosities, so that α_2 never becomes larger than a saturation value $\alpha_{\rm max}$ of the order of unity. This can have major consequences in the evolution of systems where a warped disc is present. In particular, it affects the location of the warp radius in the Bardeen–Petterson effect and therefore the spin-up (or spin-down) of supermassive black holes in the nuclei of galaxies. Additionally, we also find that while the rate of warp diffusion does not depend significantly on the detailed viscosity formulation, the rate of internal precession generated by the warp is strongly affected by it. Such effects should be considered with care when modelling the evolution of warped discs. This emphasizes the need to test the above results using different numerical schemes, and with higher resolution, in order to investigate the degree to which numerical simulations are able to provide accurate modelling of the complex fluid dynamics of warped discs.

Key words: accretion, accretion discs – hydrodynamics – instabilities.

1 INTRODUCTION

Many (perhaps most) astrophysically relevant accretion discs are expected to be twisted or warped. The torques responsible for such warping can be very different, including tidal effects of a companion star in binary systems (Larwood et al. 1996), dynamical effects during the formation of protostellar discs, general relativistic Lense–Thirring precession around a spinning black hole (Bardeen & Petterson 1975; Scheuer & Feiler 1996; Lodato & Pringle 2006), and self-induced warping caused by radiation pressure (Pringle 1996).

Observationally, warps are found both in discs which are expected to be relatively thick, such as the case of the hyperaccreting X-ray binary SS433 (Begelman, King & Pringle 2006) or, on the much less energetic side, the disc around the young star KH 15D (Chiang & Murray-Clay 2004). In some other cases, warps are also found in very thin discs, in the nucleus of the AGN NGC 4258 (Herrnstein, Greenhill & Moran 1996; Papaloizou, Terquem & Lin 1998) or in the X-ray binary Her X-1 (Wijers & Pringle 1999).

The secular evolution of such warped discs deeply affects the structure of the system. For example, the process of alignment between the spin of a black hole and the angular momentum of the disc due to the Bardeen–Petterson effect strongly depends on the effectiveness of warp diffusion in thin discs (Lodato & Pringle 2006). This can have major consequences on the spin-up or spin-down of the black hole during an accretion event, having implications also on the formation and early growth of supermassive black holes (King & Pringle 2006).

While the linear (and mildly non-linear) theory of warp propagation has been investigated extensively in the past (Papaloizou & Pringle 1983; Pringle 1992; Papaloizou & Lin 1995; Ogilvie 1999, 2000) and has been tested numerically in the case where the disc is thick enough that warp propagation is wave-like (Nelson & Papaloizou 1999, 2000), there is as yet no numerical confirmation of the diffusive warp propagation expected in the thin disc case, nor

★E-mail: giuseppe.lodato@astro.le.ac.uk

a full description of the non-linear effects that might arise when the amplitude of the warp becomes large compared to viscosity.

We consider here the propagation of warps in thin Keplerian accretion discs in the case when the disc is sufficiently viscous that the warp propagates in a diffusive manner.

We start by defining the main disc properties. We consider a thin disc, rotating with angular velocity $\Omega(R)$, with surface density $\Sigma(R)$ and angular momentum per unit area $\boldsymbol{L}(R)$. Here R should be interpreted as a 'spherical' coordinate. The local direction of $\boldsymbol{L}$ can be oriented anyhow in space, and the unit vector $\boldsymbol{l}(R) = \boldsymbol{L}(R)/L(R)$ defines its direction. If the disc is rotating around a central point mass M, then its rotation is Keplerian, with $\Omega = \sqrt{GM/R^3}$ and $L(R) = \Sigma(R)\sqrt{GMR}$.

The disc is warped whenever the direction identified by $\boldsymbol{l}$ changes with radius. We can characterize the warp amplitude with the dimensionless parameter ψ, where

$$\psi = R\left|\frac{\partial \boldsymbol{l}(R)}{\partial R}\right|. \tag{1}$$

The disc thickness is $H = c_s/\Omega$, where c_s is the sound speed, and is the scale over which density and pressure change in the local z direction. The disc aspect ratio is H/R, and we shall assume that $H/R \ll 1$.

Papaloizou & Pringle (1983) and Pringle (1992) have introduced a simple equation to describe the evolution of a warped disc, in the case where the warp propagates diffusively in the disc. As shown by Papaloizou & Lin (1995), diffusive behaviour occurs for isotropic viscosity if the disc aspect ratio $H/R < \alpha$, where α is the viscosity parameter commonly used as a measure of the (R, ϕ) (viscous) stresses in the disc (Shakura & Sunyaev 1973). In this case the warp propagation can be approximately described by the equation (Pringle 1992)

$$\begin{aligned}\frac{\partial \boldsymbol{L}}{\partial t} &= \frac{3}{R}\frac{\partial}{\partial R}\left[\frac{R^{1/2}}{\Sigma}\frac{\partial}{\partial R}(\nu_1 \Sigma R^{1/2})\boldsymbol{L}\right] \\ &+ \frac{1}{R}\frac{\partial}{\partial R}\left[\left(\nu_2 R^2\left|\frac{\partial \boldsymbol{l}}{\partial R}\right|^2 - \frac{3}{2}\nu_1\right)\boldsymbol{L}\right] \\ &+ \frac{1}{R}\frac{\partial}{\partial R}\left(\frac{1}{2}\nu_2 R|\boldsymbol{L}|\frac{\partial \boldsymbol{l}}{\partial R}\right).\end{aligned} \tag{2}$$

In this equation, the terms proportional to ν_1 describe the standard viscous evolution of a thin and flat disc, where ν_1 is the usual viscosity acting on the (R, ϕ) shear. If we use the α-parametrization, we have

$$\nu_1 = \alpha c_s H = \alpha \Omega H^2. \tag{3}$$

The terms proportional to ν_2 in equation (2) arise whenever the disc is warped and $|\partial \boldsymbol{l}/\partial R| \neq 0$. According to equation (2) the warp diffuses with a diffusion coefficient ν_2. In view of this we shall define a second parameter α_2 defined similarly so that

$$\nu_2 = \alpha_2 c_s H = \alpha_2 \Omega H^2. \tag{4}$$

It is clear that the nature of the evolution of a warped accretion disc is determined mainly by the relative values of α and α_2.

We stress that equation (2) was not derived from any hydrodynamical (or magnetohydrodynamical) equations. Rather the equation results simply from the conservation equations (mass and angular momentum), coupled with the assumption that the warp propagates in a diffusive manner. Thus there is no linear approximation required in the derivation and the equation is, in principle, applicable to warps of any amplitude, with an appropriate choice of ν_2. Thus, equation (2) merely states that the warp evolution is diffusive, with a diffusion coefficient ν_2 to be determined.

A number of authors have addressed the problem of warp diffusion. Papaloizou & Pringle (1983) considered the internal hydrodynamics of the disc, assuming an internal *isotropic* viscosity for a warp small enough to be treated as a linear perturbation (i.e. $\psi \ll H/R$), and for viscosity such that $H/R \lesssim \alpha \ll 1$. In this case the internal hydrodynamic flow is a laminar one, and is relatively straightforward to analyse (see Section 4). They found that to first order equation (2) gives the correct behaviour, along with the rather surprising result that

$$\frac{\nu_2}{\nu_1} = \frac{\alpha_2}{\alpha} = \frac{1}{2\alpha^2}. \tag{5}$$

This implies that

$$\alpha_2 = \frac{1}{2\alpha}, \tag{6}$$

and therefore that the warp diffusion coefficient is *inversely* proportional to the size of the viscosity. We discuss the physics behind this in Section 4. To next order in α there are additional terms which imply precession of the disc, and which are not included in the simple formulation of equation (2).

Ogilvie (1999) (see also Ogilvie 2000; Ogilvie & Dubus 2001) extends these approximate analytic results by use of an asymptotic expansion in terms of the small quantity H/R, but retaining the assumption of an isotropic (Navier–Stokes) viscosity. By this means he is able to take account of larger values of α and ψ and to this approximation the internal dynamics is still in the form of well-ordered, laminar flows. Ogilvie (1999) finds

$$\frac{\nu_2}{\nu_1} = \frac{1}{2\alpha^2}\frac{4(1+7\alpha^2)}{4+\alpha^2}, \tag{7}$$

when $\psi \ll 1$ and also gives higher order corrections with terms in ψ^2. He also finds additional precessional terms, which are generally of higher order than the terms already included (we discuss this further in Section 3.4).

None of these studies takes into account the fact that viscosity in real accretion discs is most likely not a simple isotropic Navier–Stokes viscosity. It is generally believed (see e.g. Balbus & Hawley 1998) that the mechanism responsible for angular momentum transport in discs (corresponding to ν_1) is magnetohydrodynamics (MHD) turbulence, driven by the magnetorotational instability. An attempt at estimating ν_2 has been made by Torkelsson et al. (2000) in a numerical shearing box simulation. It has become evident recently, however, that the results of such simulations are somewhat problematic (Fromang & Papaloizou 2007; King, Pringle & Livio 2007; Pessah, Chan & Psaltis 2007). In addition, as discussed by Pringle (1992), there is no particular reason to assume that the mechanism which damps the warp (corresponding to ν_2) is the same. In addition, for large (astrophysically significant) warps the internal motions can become sufficiently large, with relative supersonic velocities, that a number of authors have argued that they are likely to be unstable (Coleman & Dopita 1992; Gammie, Goodman & Ogilvie 2000) and so result in enhanced dissipation.

In the opposite regime of thick discs, or of lower viscosity, the warp evolves to first order as a non-dispersive bending wave (Papaloizou & Lin 1995). The equations of motion for a wave in the case where the disc is Keplerian and nearly inviscid are (Lubow & Ogilvie 2000; Lubow, Ogilvie & Pringle 2002)

$$\Sigma R^3 \Omega \frac{\partial \boldsymbol{l}}{\partial t} = \frac{\partial \boldsymbol{G}}{\partial R}, \tag{8}$$

$$\frac{\partial \boldsymbol{G}}{\partial t} + \alpha\Omega\boldsymbol{G} = \Sigma R^3 \Omega \frac{c_s^2}{4}\frac{\partial \boldsymbol{l}}{\partial R}, \tag{9}$$

where $\boldsymbol{G}$ is the disc internal torque. The corresponding dispersion relation is then (Nelson & Papaloizou 1999)

$$\omega(\omega - \mathrm{i}\alpha\Omega) = \frac{c_s^2 k^2}{4}, \tag{10}$$

where ω is the wave frequency, k the wavenumber and c_s the sound speed. The solution for ω is

$$\omega = \frac{1}{2}\left\{\mathrm{i}\alpha\Omega \pm \left[c_s^2 k^2 - \alpha^2\Omega^2\right]^{1/2}\right\}. \tag{11}$$

Thus the above relation shows that in the absence of viscosity ($\alpha = 0$) a bending wave propagates at half the sound speed. When $\alpha \geqslant Hk$, i.e. when $\alpha \geqslant 2\pi H/\lambda$, where λ is the wavelength of the perturbation, we see that ω is purely imaginary, and wave-like propagation no longer occurs. Propagation becomes purely diffusive in the limit $|\omega| \ll \alpha\Omega$, in which case we obtain

$$\frac{\omega}{\mathrm{i}\alpha\Omega} = \left(\frac{c_s k}{2\alpha\Omega}\right)^2 \ll 1. \tag{12}$$

Thus pure diffusion occurs when $\alpha \gg \frac{1}{2}Hk = \pi H/\lambda$. The boundary between the purely diffusive and purely wave-like propagation regimes is not a sharp one. For convenience we shall take the transition between diffusive and wave-like regimes to occur at the value $\alpha = \alpha_c$ when the real and imaginary parts of ω are equal $\omega_R = \omega_I$. Thus the critical value of α is given by

$$\alpha_c = \frac{1}{\sqrt{2}}Hk. \tag{13}$$

In this paper we investigate the hydrodynamics of diffusive warp propagation (i.e. $\alpha > \alpha_c$) using numerical simulations. In particular, we use smoothed particle hydrodynamics (SPH). Such a technique has been used in some of the most accurate investigations of warp propagation to date (Larwood et al. 1996; Nelson & Papaloizou 1999, 2000) and is particularly suited to the treatment of complex and variable geometries, like that of a warped disc. However, as we will further discuss below, some numerical effects, e.g. related to the implementation of viscosity, might play a role and we stress the importance of conducting similar analyses with different codes, especially in view of simulating a warped disc that evolves under the action of MHD instabilities, which are not taken into account here. The early investigations by Nelson & Papaloizou (1999, 2000) have focused on the thick-disc regime, where the warp propagates as a bending wave, but have already noticed some dissipational effects. In this respect, the present work can be seen as complementary to these previous ones, since we here focus on the thin-disc regime, where the character of warp propagation is expected to differ substantially from the thick-disc case.

The paper is organized as follows. In Section 2 we present the numerical set-up, and we present the results in Section 3. In Section 4 we present a simplified discussion of the physics of diffusive warp propagation, and use this analysis to interpret our results. We discuss the implications and limitations in Section 5.

2 NUMERICAL SET-UP

We have performed a set of three-dimensional SPH simulations of warped discs. SPH is a Lagrangian hydrodynamic scheme (Gingold & Monaghan 1977; Lucy 1977; Benz 1990; Monaghan 1992), in which the gas disc is modelled with N particles. For most of our simulations we have used one or two million particles (these are some of the highest resolution SPH disc simulations to date).

In the following we use code units in which the gravitational constant $G = 1$, the central point mass $M = 1$, so that at a radius $R = 1$ in code units, the dynamical time is $\Omega^{-1} = 1$.

We set up our warped disc by placing the gas particles in Keplerian orbits around a central point mass $M = 1$ (in code units), modelled as a sink particle (Bate, Bonnell & Price 1995), with accretion radius $R = 0.5$ in code units. We distribute them in such a way that the disc has a prescribed initial surface density profile, as described below. We assign each particle a radius-dependent sound speed c_s, so as to attain the desired temperature profile (see below). The particles are then distributed in z so as to attain a Gaussian density profile in the vertical direction, with thickness $H = c_s/\Omega$. We then tilt the orbit of each particle in such a way that the components of the unit vector $\boldsymbol{l}$ are given by

$$l_x = \begin{cases} 0 & \text{for } R < R_1, \\ \dfrac{A}{2}\left[1 + \sin\left(\pi\dfrac{R - R_0}{R_2 - R_1}\right)\right] & \text{for } R_1 < R < R_2, \\ A & \text{for } R > R_2, \end{cases} \tag{14}$$

$$l_y = 0, \tag{15}$$

$$l_z = \sqrt{1 - l_x^2}, \tag{16}$$

where $R_1 = 3.5$ and $R_2 = 6.5$ in code units, and $R_0 = (R_1 + R_2)/2$. The initial shape of the warp is plotted in Fig. 1. The warp amplitude ψ is then

$$\psi = R\left|\frac{\partial \boldsymbol{l}}{\partial R}\right| = \frac{R}{l_z}\frac{\partial l_x}{\partial R} \tag{17}$$

the maximum of which is attained at $R \approx R_0$ and is given by

$$\psi_{\max} \approx \frac{\pi R_0 A}{2(R_1 - R_2)} = 2.62A. \tag{18}$$

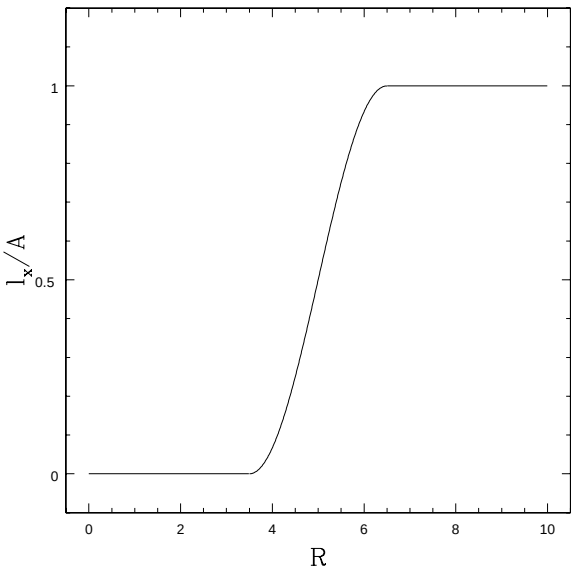

Figure 1. Initial profile of the x component of the unit vector $\boldsymbol{l}$ in our SPH simulations. Note that the y component is initially zero, so that the initial warp has no twist.

Table 1. Summary of the main physical properties of the simulations carried out. Here H/R refers to the value calculated at $R = R_0$. See text (Section 3) for the definition of the parameter f and for details of the calibration of the disc viscosity parameter α. Note that $\alpha_2 = f/2\,\alpha$.

Simulation	H/R	No. of gas particles	$\psi_{\rm max}$	α	f	α_2	α_3	$\langle h\rangle/H$	VS	$\alpha_{\rm SPH}$
S0	0.0133	2×10^6	0.026	0.28	1	1.78	−0.51	0.6	On	15
S0b	0.0133	2×10^6	0.026	0.28	1	1.78	0.08	0.6	Off	7.5
S1	0.0133	2×10^6	0.026	0.23	1	2.17	−0.46	0.6	On	10
S1b	0.0133	2×10^6	0.026	0.23	1	2.17	0.17	0.6	Off	5
S2	0.0133	2×10^6	0.026	0.18	1	2.77	−0.72	0.6	On	7.5
S3	0.0133	2×10^6	0.026	0.15	0.85	2.83	−0.6	0.6	On	5
S4	0.0133	2×10^6	0.026	0.14	0.8	2.85	0.22	0.6	Off	2.5
S5	0.0133	2×10^6	0.026	0.09	0.6	3.33	−0.63	0.6	On	2.5
S6	0.0133	2×10^6	0.026	0.07	0.42	3	0.21	0.6	Off	1.7
S7	0.0133	2×10^6	0.026	0.05	0.38	3.8	0.2	0.6	Off	1
S8	0.0133	2×10^6	1.3	0.26	0.75	1.44	0.52	0.6	Off	5
S9	0.0133	2×10^6	1.3	0.1	0.6	3	−0.17	0.6	On	2.5
S10	0.0334	10^6	0.026	0.1	–	–	–	0.4	On	10
S11	0.0334	10^6	0.026	0.08	–	–	–	0.4	On	7.5
S12	0.0334	10^6	0.026	0.06	–	–	–	0.4	On	5
S13	0.0334	10^6	1.3	0.08	–	–	–	0.4	On	7.5
S14	0.0668	10^6	1.3	0.04	–	–	–	0.1	On	5

The disc extends from $R_{\rm in} = 0.5$ to $R_{\rm out} = 10$, with a surface density profile, Σ, given by

$$\Sigma(R) = \Sigma_0 R^{-p}\left(1-\sqrt{\frac{R_0}{R}}\right). \tag{19}$$

Note that the density normalization Σ_0 does not play a role in our simulations, since we do not include the disc self-gravity in the computation. The parameter p is set to $p = 3/2$. The simulations we perform are locally isothermal, with a sound speed $c_{\rm s}$, given by

$$c_{\rm s} = c_{\rm s,0} R^{-q}, \tag{20}$$

where $q = 3/4$ and where the normalization $c_{\rm s,0}$ determines the disc thickness.

In order to model the viscous evolution of the disc, we use the SPH artificial viscosity formalism (Monaghan 1992). It has been shown (Artymowicz & Lubow 1994; Murray 1996) that artificial viscosity in SPH can mimic the behaviour of an α-viscosity, with

$$\alpha \propto \alpha_{\rm SPH}\frac{\langle h\rangle}{H}, \tag{21}$$

where $\alpha_{\rm SPH}$ is the artificial viscosity coefficient, $\langle h\rangle$ is the average smoothing length and H is the disc thickness. Our set-up has been chosen in such a way that the disc thickness is uniformly resolved at different radii. Indeed, the disc thickness H scales with radius as

$$H = \frac{c_{\rm s}}{\Omega} \propto R^{3/2-q}, \tag{22}$$

and we expect the average smoothing length at one radius to scale as

$$\langle h\rangle \propto \rho^{-1/3} \propto \left(\frac{\Sigma}{H}\right)^{-1/3} \propto R^{(p-q)/3+1/2}. \tag{23}$$

Thus, by choosing $p = 3/2$ and $q = 3/4$, we have that $H \propto \langle h\rangle \propto R^{3/4}$. This then produces a disc with a constant α, the magnitude of which can be adjusted by varying the SPH artificial viscosity parameter $\alpha_{\rm SPH}$. Additionally, since $\nu_1 = \alpha\Omega H^2$, and $H \propto R^{3/4}$, we also expect that the simulations be characterized by a constant viscosity ν_1.[1] As for the quadratic term in the standard formulation of SPH artificial viscosity (the 'β'-term), we have only included it in simulations for which the 'viscous switch' is on (see below), in which cases we have adopted the common practice of setting $\beta_{\rm SPH} = 2\alpha_{\rm SPH}$.

We have performed several simulations, varying the disc aspect ratio H/R, the viscosity α (through varying the SPH artificial viscosity $\alpha_{\rm SPH}$, see Section 3 below for details on how we calibrate the viscosity) and the peak warp amplitude ψ. The main parameters of our simulations are summarized in Table 1. The ninth column of Table 1 shows the (radius-independent) ratio of the azimuthal and vertical average of the smoothing length h and the disc thickness H, which also demonstrates that we resolve the vertical structure moderately well in the simulations. Note that this column shows a vertical average of the smoothing length h, including the contribution of particles at high z which have a smaller density and hence a larger h. The actual value of h in the bulk of the disc can be significantly smaller than the average. As a further check of the resolution achieved in our simulations, we plot in Fig. 2 the azimuthally averaged vertical density profile for simulations S0 to S9 (see Table 1), at two different radii, $R = 1$ (left-hand panel) and $R = 3$ (right-hand panel). The solid line shows the theoretical profile derived applying the standard hydrostatic balance condition, while the dashed and dotted lines (almost exactly coincident) show the value of the density as computed from the SPH scheme at two times, $t = 10$ (dashed) and $t = 30$ (dotted) code units. We can clearly see that the SPH estimates follow nicely the predicted profile, deviating from it only at vertical height $z \gtrsim 2H$, where the density is already a factor of 0.2 smaller than the peak.

As can be seen from Table 1 we have considered three different values for the disc thickness. Most of our simulations have $H/R \approx 0.0133$, a few have $H/R \approx 0.0334$ and only one had a relatively large thickness of $H/R \approx 0.0668$. The critical value of α below which wave propagation is expected to occur is then $\alpha_{\rm c} = 0.05$, 0.12 and 0.25, respectively. It can be then easily seen that the thickest

[1] We thank Gordon Ogilvie for suggesting this set-up to us.

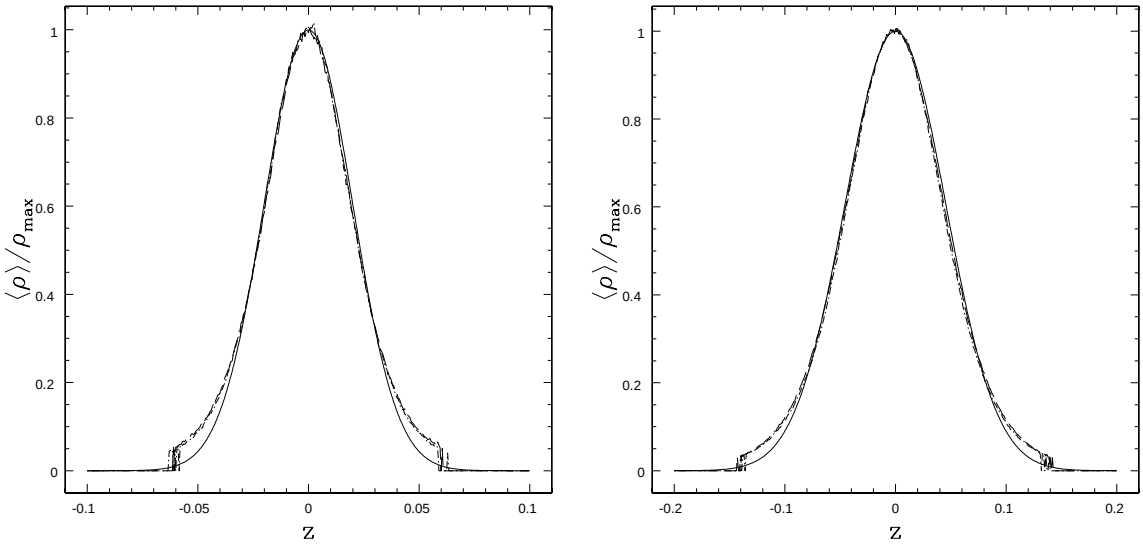

Figure 2. Azimuthally averaged vertical density profile for simulations S0 to S9, at $R = 1$, where the disc thickness $H = 0.02$ (left-hand panel) and $R = 3$, where $H = 0.045$ (right-hand panel). The solid line shows the theoretical Gaussian profile expected in vertical hydrostatic balance, while the dashed and dotted lines (almost exactly coincident) show the density evaluated from the SPH code at $t = 10$ and 30 code units, respectively. Deviations from the expected profile only occur at a height $z \gtrsim 2H$, where the density has decreased by a factor of 0.2.

case we consider falls in the wave-propagation regime, while the thinnest case (the majority of simulations) falls in the diffusion regime. The intermediate thickness is marginal, and wave propagation with significant dissipation is expected.

2.1 On modelling disc viscosity in SPH

In this paper, we have used the internal SPH viscosity in order to simulate a (Navier–Stokes) viscosity in the disc. This is clearly an idealization, since there is no a priori expectation that real disc viscosity in any way resembles Navier–Stokes. In practice accretion discs transport is likely to be dominated by other forms of stress (e.g. due to the magnetorotational instability). But at least this provides some insight on the evolution of the warp in this specific case, and provides some comparison with previous analytic work.

However, care should be taken when using the SPH artificial viscosity to model a Navier–Stokes viscosity. Standard implementations of SPH adopt the so-called 'viscous switch', so that viscous forces are only active when acting on approaching particles, and vanish for receding particles. Clearly, if we want to simulate something approximating a Navier–Stokes viscosity we should turn the 'viscous switch' off. Artymowicz & Lubow (1994) and Murray (1996) have already remarked on this.

Because it is unclear how the real, physical disc viscosity behaves, we have run simulations with and without the 'viscous switch'. The column 'VS' is Table 1 indicates the simulations that had the switch on or off (note that obviously in order to reproduce the same physical viscosity coefficient α, a much smaller value of $\alpha_{\rm SPH}$ – roughly half – is needed when the viscous switch is off, as shown in Table 1). This enables us to directly check the impact of using the viscous switch or not in the evolution of our warped discs. As we discuss below (Section 3.3), the effects on the evaluation of the warp diffusion coefficient (i.e. on the diffusion/damping of the warp) are minor, if not negligible. There is however a strong sensitivity in the rate, and indeed direction, of internal precession induced by the warp.

3 RESULTS

In this section we describe the main results of our simulations. Our general procedure for the analysis is relatively simple. We first divide the radial range of the simulation in a series of annuli at different radii R. From the output of the SPH simulation we then compute the surface density $\Sigma(R)$ and the azimuthal and vertical average of the three components of the unit vector $\boldsymbol{l}$ as functions of time. We then compare the evolution of these quantities with the evolution predicted either by equation (2) (for the thinnest cases), or by equations (8) and (9) (for the thick cases).

3.1 Wave-like propagation in the thick-disc case

As mentioned above, we expect the warp to propagate as a bending wave in the thickest of our simulations, and possibly also the intermediate thickness ones. This is indeed confirmed by our simulations. As an example, we show in Fig. 3 the evolution of simulation S11. The left-hand panel shows the evolution of the surface density Σ (solid lines), compared to the evolution predicted by a simple viscous surface density evolution with $\alpha = 0.08$. The right-hand panel shows the evolution of the x component of $\boldsymbol{l}$ (solid lines) compared to the evolution predicted from equations (8) and (9). Note that in order to obtain a good fit to the simulations it is essential also to include the dissipative term in equation (9), i.e. the second term on the left-hand side of the equation, since a pure wave evolution does not fit the data. We also note that the same evolution could also in principle be fitted (at least over the limited time span covered by the simulation) with a diffusive warp propagation model, but where the warp diffusion coefficient is taken to be much smaller than the value predicted from the linear theory, i.e. $\alpha_2 \approx 2.5 \ll 1/2\alpha$.

3.2 Diffusive propagation in the thin-disc case

For our thinnest disc case we expect the warp to propagate diffusively, according to equation (2). We have then solved equation (2) numerically using the techniques described in detail in Pringle (1992) and in Lodato & Pringle (2006). The model described in

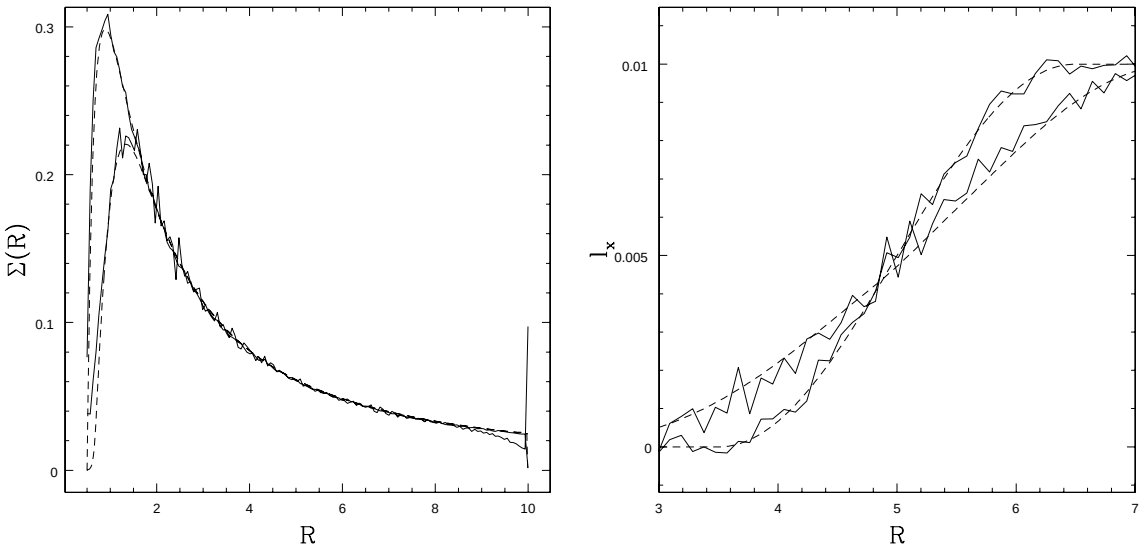

Figure 3. Evolution of simulation S11. The solid lines refer to the azimuthal and vertical average of the SPH simulation, while the dashed lines show the evolution of the corresponding initial conditions obtained by applying equations (8) and (9) for the warp, while the surface density is evolved using a viscosity parameter $\alpha = 0.08$. The left-hand panel shows the evolution of the surface density Σ, while the right-hand panel shows the evolution of l_x. The different lines refer to $t = 0$ and 155 (in units of the dynamical time at $R = 1$).

equation (2) contains two free parameters, namely the two viscosities ν_1 and ν_2, and we adjust these in order to match the evolution of the simulation. In particular, the surface density Σ is most sensitive to the value of the viscosity ν_1, while the evolution of the component l_x of the unit vector $\boldsymbol{l}$ is most sensitive to the value of ν_2. We therefore use these two quantities separately to determine the two parameters. To be sure, the evolution of Σ does also depend on ν_2 (Pringle 1992). However, this effect scales quadratically with the warp amplitude and can be generally neglected in most of our simulations (with some exceptions, as shown below).

In practice, we determine the value of α and the value of a parameter f, which is a measure of the deviation of ν_2 from the value expected from the linear theory. Thus f is defined by

$$\frac{\nu_2}{\nu_1} = \frac{f}{2\alpha^2}. \tag{24}$$

The fifth and sixth columns of Table 1 show the measured values of α and f for all of our simulations. It can be seen that we are able to span a range of α that goes from 0.05 to 0.28, which is roughly a factor of 7. Only for the three largest values of α does the measured value of f agree with the linear estimate, while for most other cases the diffusion coefficient ν_2 is smaller than predicted by linear theory.

Note that, with regard to the evaluation of the warp diffusion coefficient, the simulations which have an implementation of viscosity that more closely resembles a Navier–Stokes viscosity (i.e. viscous switch off) do not show significant differences with respect to the corresponding ones with the viscous switch turned on. Simulations S0 and S0b and S1 and S1b, that have the same estimated value of α, also share the same warp diffusion coefficient. Simulations S3 and S4, which have very similar values of α, also have a similar diffusion coefficient. Note that this agreement encompasses the whole range of viscosities that we probe in the thinnest disc configuration, extending from high values of α, for which the warp diffusion rate agrees with the linear theory, down to lower values, where some non-linear effects start to play a role.

Fig. 4 shows one example of our analysis, corresponding to the case where $H/R = 0.0133$, $\alpha = 0.18$ and $\psi_{\max} = 0.026$ (simulation S2). The left-hand panel shows the evolution of Σ, while the right-hand panel shows the evolution of l_x. The solid lines refer to the results of the SPH evolution at two different times, $t = 0$ and 465 in code units (where the unit time is the dynamical time at $R = 1$), while the dashed lines show the evolution of the simple model of equation (2). As can be seen, the evolution of the two quantities is well reproduced by the model, therefore demonstrating numerically for the first time the validity of the diffusive model for warp propagation in this regime. In this particular case, not only does the warp evolve diffusively, but the value of the diffusion coefficient agrees with the expectations from the linear theory, i.e. we measure $f = 1$.

Fig. 5 shows the evolution of simulation S6. This simulation is also well fitted by a diffusive model, except that in this case, although the value of $\alpha = 0.07$ is above the critical value so that diffusive propagation is expected (in this case $\alpha_c \simeq 0.05$), the required value of $\alpha_2 \approx 3$ is significantly below the value expected from the linear theory $1/2\alpha \approx 7.14$. To be sure that wave-propagation effects do not play a significant role here, we have also tried to fit the evolution of this simulation with a wave-propagation model, as done in the previous section. The results are shown in Fig. 6. It can be seen that in this case a wave-propagation model (including the effects of viscosity) does not reproduce the results of the simulation.

Most of our simulations have a low-amplitude warp, with $\psi \approx 0.026$. However, we have also run some simulations with $\psi \sim 1$. In the thin-disc case, these simulations are S8 and S9, for which $\psi \approx 1.3$. Simulation S8 has $\alpha = 0.26$, for which the corresponding low-amplitude simulations follow the linear predictions for α_2 (equation 6). Simulation S9 instead has $\alpha = 0.1$, for which the low-amplitude simulation is already in the saturated regime for α_2. In both cases the diffusion coefficient is found to be smaller than the value predicted from equation (6) and we measure $f = 0.75$ for S8 and $f = 0.6$ for S9. The results for simulation S8 thus show that increasing the warp amplitude leads to a marginal reduction of the diffusion coefficient. On the other hand, in the case of simulation S9, with $\alpha = 0.1$ for which a low-amplitude warp is already enough to induce a reduction of α_2 with respect to linear theory, a further increase of ψ does not lead to a significant further reduction of α_2.

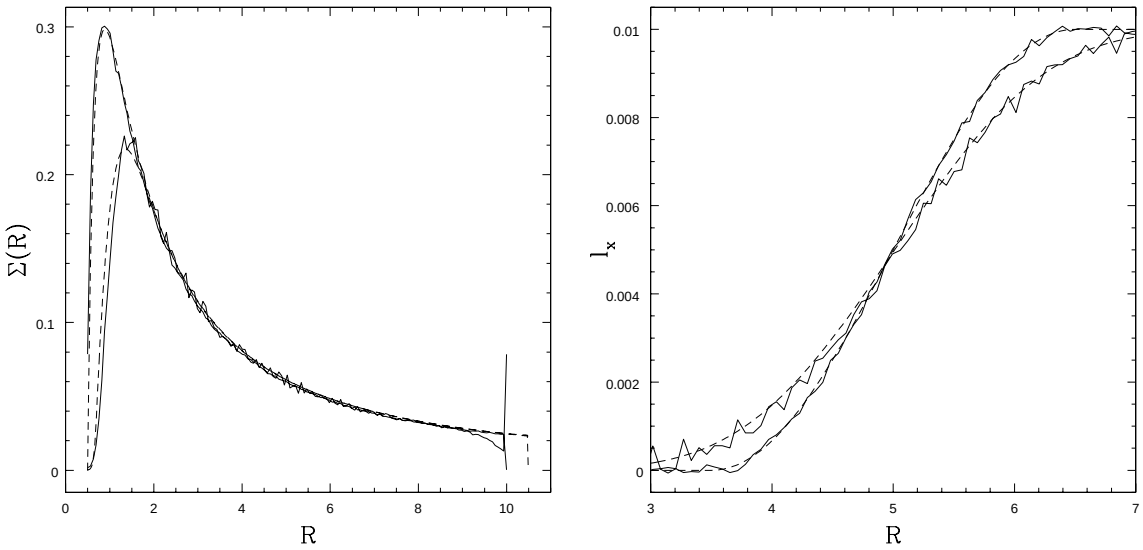

Figure 4. Evolution of simulation S2. The solid lines refer to the azimuthal and vertical average of the SPH simulation, while the dashed lines show the evolution of the corresponding initial conditions obtained by applying equation (2), with the following parameters: $\alpha = 0.18$ and $f = 1$. The left-hand panel shows the evolution of the surface density Σ, while the right-hand panel shows the evolution of l_x. The different lines refer to $t = 0$ and 465 (in units of the dynamical time at $R = 1$).

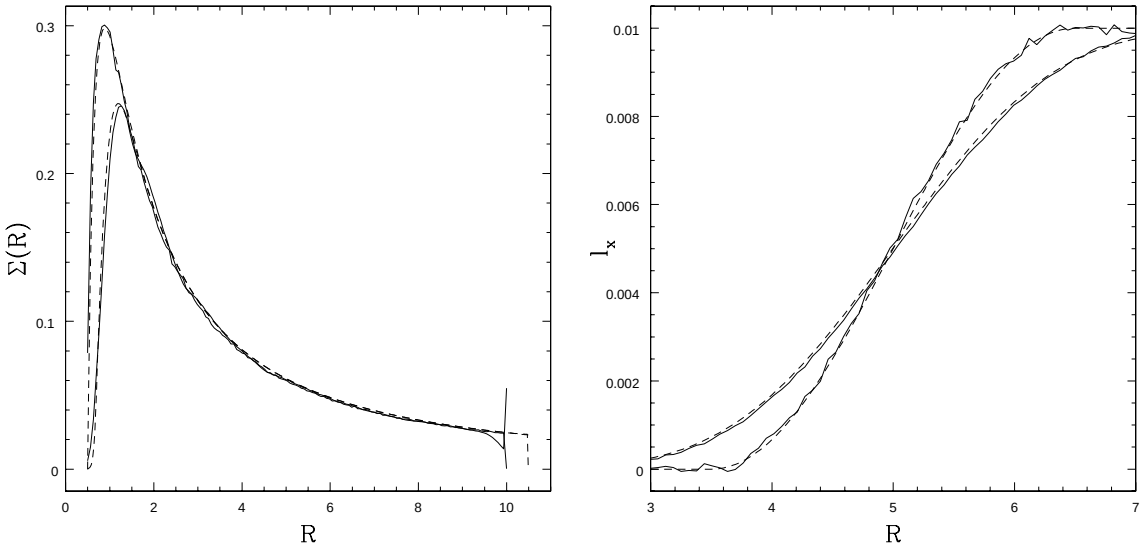

Figure 5. Evolution of simulation S6. The solid lines refer to the azimuthal and vertical average of the SPH simulation, while the dashed lines show the evolution of the corresponding initial conditions obtained by applying equation (2), with the following parameters: $\alpha = 0.07$ and $f = 0.42$. The left-hand panel shows the evolution of the surface density Σ, while the right-hand panel shows the evolution of l_x. The different lines refer to $t = 0$ and 550 (in units of the dynamical time at $R = 1$).

These large amplitude simulations are also interesting because they reveal the effects of the warp diffusion term on the evolution of the disc surface density. Fig. 7 shows the evolution of simulation S8 (solid line) along with the evolution of the simple diffusive model of equation (2) (dashed line). Note how the model reproduces well the inflection of the surface density close to the warp location. The inflection is due to the effect of ν_2 on the evolution of Σ, as mentioned earlier, and shown in Pringle (1992). In contrast with the previous low-amplitude simulations, in this case, where the warp amplitude is large, this effect does play a role. Such effect has been described clearly in Pringle (1992) and more recently in Lodato & Pringle (2006). Note that such dissipative effects cannot be reproduced by a purely wave-like warp propagation.

3.3 The diffusion coefficients

Each one of the high-resolution simulations described in the previous section is quite demanding in terms of computing time, and we could only run a few such simulations. As a result, we could only obtain a partial coverage of the relevant parameter space. Even so, we can still draw some interesting conclusions from the limited available data.

First, we find that the evolution of the disc is well described by equation (2), and the numerical results can be fitted by just varying the parameters α and α_2. We stress that we do not perform an actual statistical fit of the viscosity coefficients, but simply choose them so as to match the evolution of the numerical simulations. We estimate

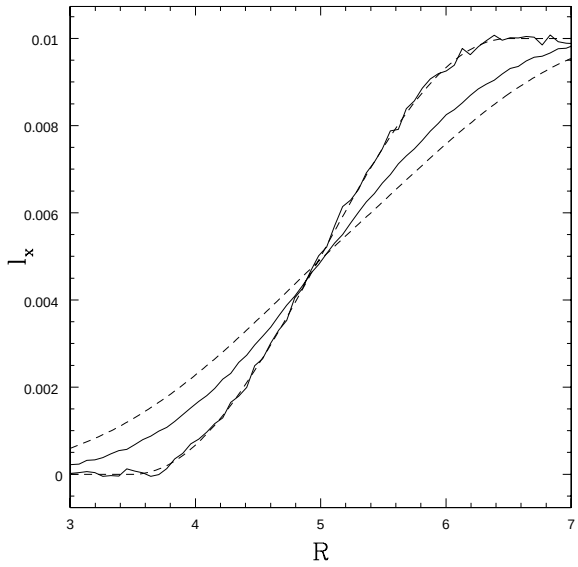

Figure 6. Evolution of simulation S6. The solid lines refer to the azimuthal and vertical average of the SPH simulation, while the dashed lines show the evolution of the corresponding initial conditions obtained by applying equations (8) and (9), with $\alpha = 0.07$. The different lines refer to $t = 0$ and 550 (in units of the dynamical time at $R = 1$).

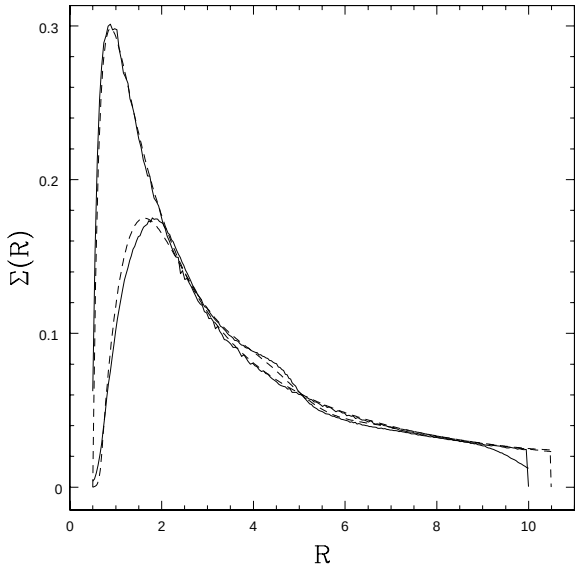

Figure 7. Evolution of simulation S8. The solid line shows the results of the SPH simulations, while the dashed line shows the diffusive evolution, according to equation (2). The two snapshots refer to $t = 0$ and 870 in code units. The inflection in the surface density is caused by the effect of ν_2 on the surface density, as discussed by Pringle (1992).

that the typical uncertainty on these parameters is ≈7 per cent for α and ≈10 per cent for α_2.

Fig. 8 shows the values of the diffusion coefficient for the warp, as obtained from all of our thin-disc simulations, for which propagation of warp occurs diffusively. The solid symbols refer to the case where the viscous switch is turned off (that should be closer to a Navier–Stokes viscosity), while the open symbols refer to the case where the viscous switch is on. For the two simulations with the highest α, the point refers to both cases, as the results were identical. The circles refer to the high-amplitude simulations. As an example, we

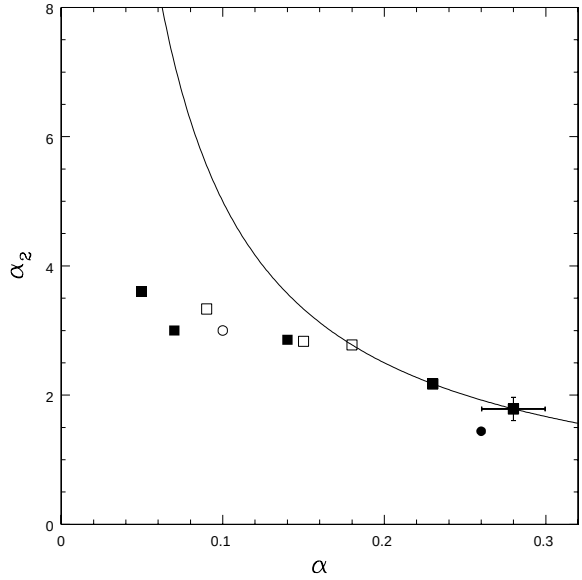

Figure 8. Results of the numerical simulations. The points indicate the values of the diffusion coefficient α_2 as a function of the viscosity coefficient α. The solid symbols refer to simulations that do not use the 'viscous switch' and should thus have a viscosity more closely approximating Navier–Stokes. The open symbols do use the viscous switch. The squares refer to the small warp amplitude case $\psi_{\max} \approx 0.026$, while the circles refer to the large amplitude case $\psi_{\max} \approx 1.3$. The error bars shown represent the typical uncertainties on the diffusion coefficients. The solid line shows the expected value of α_2 from the linear theory. It is evident that our simulations reproduce the expected results from linear theory for values of $\alpha > 0.16$. Below this value we find that α_2 appears to saturate at a value around $\alpha_{\max} \sim 3$–4.

also show for one point the typical uncertainties of the estimated parameters.

It can be seen that the points follow the expected relation $\alpha_2 = 1/2$ α at large α, but as α decreases, the value of α_2 begins to deviate from the theoretical relation and appears to saturate at a value of around $\alpha_{\max} \sim 3$–4. However, perhaps surprisingly, comparison of runs S5 and S9 shows that we do not observe any dependency of the saturation value on the warp amplitude.

3.4 Precession

Our simulations also display some small precessional effects. This is shown in Fig. 9, that shows the evolution of the y component of the angular momentum of the disc, $l_y(R)$. This is initially set to be zero (see equation 15) but it then grows due to internal precessional torques. Such torques are not accounted for in the diffusion model by Pringle (1992), but they are present in the full linear theory (e.g. Ogilvie 1999). In interpreting our results we have added such terms in our simple diffusion model, by adding a term on the right-hand side of equation (2), in the form of (see Ogilvie 1999)

$$\left.\frac{\partial \boldsymbol{L}}{\partial t}\right|_{\rm prec} = \frac{1}{R}\frac{\partial}{\partial R}\left(\nu_3 R|\boldsymbol{L}|\boldsymbol{l}\times\frac{\partial \boldsymbol{l}}{\partial R}\right), \qquad (25)$$

where we have introduced a third coefficient ν_3 related to precessional effects (with a corresponding $\alpha_3 = \nu_3/\Omega H^2$). The solid lines in Fig. 9 show the evolution of the SPH simulations, while the dashed lines refer to the simple model (including precession). The two simulations shown in Fig. 9 are S1b (left-hand panel) and S1 (right-hand panel) which have the same α and α_2 but use a different implementation of viscosity, so that S1 uses the viscous switch, while S1b

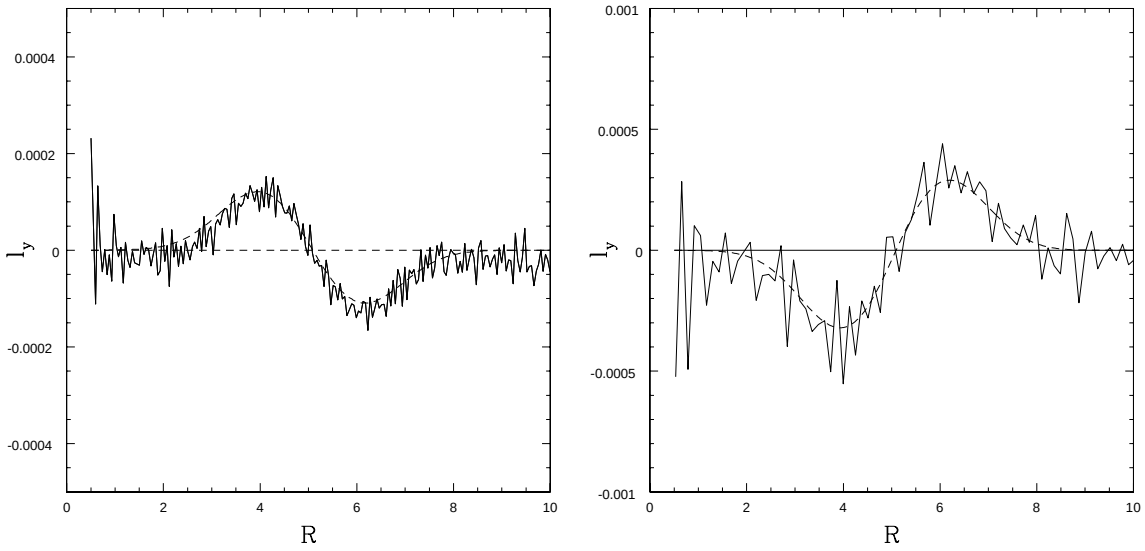

Figure 9. Evolution of the component l_y of the unit vector $\boldsymbol{l}$. Initially $l_y = 0$ and it is the precessional torques, neglected in equation (2), which cause l_y to evolve. Left-hand panel: simulation S1b (with the viscous switch turned off). Here the precession occurs in the direction predicted by the linear theory, but with a smaller precession rate. The solid line represents the results of the SPH simulation, while the dashed line represents the result of a simple diffusion model including a precessional term, with $\alpha_3 \approx 0.17$. The curves refer to $t = 825$ (in units of the dynamical time at $R = 1$). Right-hand panel: same plot for simulation S1, which has the same α and α_2 as S1b, but the viscous switch is on. Here precession occurs in the opposite direction and the best diffusion/precession model able to reproduce the results has $\alpha_3 \approx -0.46$. Here the curves refer to $t = 840$ (in units of the dynamical time at $R = 1$).

does not. The warp evolution of these two simulations agrees with the predictions of linear theory for the evolution of the warp. They do not, however, agree with linear theory with regard to disc precession. Moreover, there is an obvious difference between the two cases in that precession occurs in different directions. In order to model the evolution, we therefore require a negative α_3 term in the case of S1 and a positive α_3 for S1b. Note that the linear analytic theory, using an *isotropic* Navier–Stokes viscosity predicts a positive ν_3 with magnitude given by $\alpha_3 = 3/4$ (Papaloizou & Pringle 1983; Ogilvie 1999). The resulting values of α_3 for the simulations where we measure precession are given in Table 1. None of our simulations agrees with the analytic results.

Note that in all cases α_3 is much smaller than α_2, indicating that precession occurs on a much longer time-scale than the time-scale for diffusion and/or damping of the warp. This implies that, since internal precession is induced by the warp, it is unlikely to play any role in the disc dynamics, because by the time it starts to be important, the warp has already been diffused out, at least in the case where there is no strong external torque to enforce a given warped shape.

4 DISCUSSION

In this section we discuss the outcome of our numerical simulations and compare them with the predictions of the approximate analytic theories. Our general finding is that for values of $\alpha \geqslant 0.16$, the value of α_2 follows the simple theoretical prediction that $\alpha_2 = 1/2\ \alpha$. However, for lower values of α our simulations indicate that the value of α_2 seems to saturate at an upper limit of $\alpha_2 = \alpha_{\max} \sim 3$–4.

4.1 The theory of the simple α_2 –α relation

In order to aid theoretical understanding of the processes involved, we first introduce a simple, physical model to describe the diffusive evolution of a warp in thin, viscous discs. This model essentially reproduces the more rigorous analysis of Papaloizou & Pringle (1983), describing the main physical processes in a simple and intuitive way.

The evolution of the warp is controlled essentially by hydrodynamical processes taking place inside the disc. The main point is that a warp, coupled with the vertical stratification (with typical scale-height H) in a thin disc, induces a horizontal pressure gradient which depends on vertical height z (see Fig. 10). Thus, as a fluid element orbits in the disc with a frequency Ω, it experiences a horizontal (radial) pressure force, which oscillates at the same frequency Ω. The crucial point is that for a Keplerian disc this forcing term is resonant with the epicyclic motion, since the epicyclic frequency $\kappa = \Omega$ for a Keplerian disc. Hence the presence of the warp excites strong horizontal epicyclic motions within the disc. The magnitude

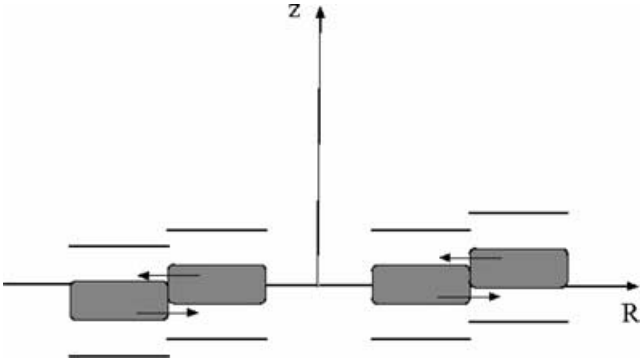

Figure 10. Schematic view of a warped disc. The shaded areas indicate regions of higher pressure. The arrows indicate the direction of the horizontal pressure gradients induced by the warp. As a fluid element orbits around the centre, it feels an oscillating radial pressure gradient, whose amplitude is a linear function of the height z.

of the induced pressure gradient is given roughly by

$$\frac{\partial p}{\partial R} \sim \frac{\partial p}{\partial z}\psi \sim \frac{p\psi}{H}. \tag{26}$$

Thus the corresponding force term in the horizontal momentum equation is

$$\frac{1}{\rho}\frac{\partial p}{\partial R} \sim \frac{c_s^2\psi}{H} \sim H\Omega^2\psi, \tag{27}$$

where we have also used $p \sim c_s^2\rho$.

As is shown in more detail in Papaloizou & Lin (1995) the forcing term varies linearly with z, and therefore excites a response, e.g. in the radial velocity field which takes the approximate form

$$v_R = v_\perp\left(\frac{z}{H}\right)\cos\phi. \tag{28}$$

Here ϕ is the azimuthal angle in the disc, and $v_\perp$ denotes the induced horizontal velocity in the radial direction at the disc 'surfaces' $z = \pm H$. If we let $x(t)$ be the radial Lagrangian displacement of a disc particle at the disc surface relative to an unperturbed disc particle on a circular orbit, then this implies that

$$x(t) = \left(\frac{v_\perp}{\Omega}\right)\sin\Omega t. \tag{29}$$

Then the disc particle at position $x(t)$ is subject to three forces: a restoring force which gives rise to the epicyclic frequency $\kappa = \Omega$, a damping force due to some form of viscous dissipation, and a pressure force caused by the warp with amplitude given by equation (27). Thus $x(t)$ obeys an equation of the form

$$\ddot{x} + \frac{\dot{x}}{\tau} + \Omega^2 x = R\Omega^2\left(\frac{\psi H}{R}\right)\cos\Omega t. \tag{30}$$

Here the amplitude of the forcing term on the right-hand side is taken from equation (27). The third term on the left-hand side is the epicyclic restoring force. The second term on the left-hand side is a damping term, where we have introduced a damping time-scale τ, which describes the viscous damping of the horizontal shear motion (described in equation 28) induced by the warp. If the horizontal shear motion is damped by a kinematic viscosity ν_z then we have simply that

$$\tau \sim \frac{H^2}{\nu_z}. \tag{31}$$

(Note that the typical length-scale of the horizontal shear is H, rather than R, hence the difference between the above formula and the corresponding one associated with the viscous time-scale in a differentially rotating disc, $t_{\rm visc} \sim R^2/\nu_1$).

If we make the further assumption (which, as we have stressed, is not necessarily true for a disc) that the viscosity is isotropic, so that $\nu_z = \nu_1$, we obtain

$$\tau \sim \frac{H^2}{\nu_1} = \frac{1}{\alpha\Omega}. \tag{32}$$

In line with our expectations (equation 29) we look for a solution to equation (30) in the form

$$x(t) = a\sin\Omega t, \tag{33}$$

where now a is the amplitude of the horizontal motions at the disc surfaces $z = \pm H$. Substituting (33) into (30), we find a solution for the amplitude of the horizontal motion a

$$a = \psi H(\Omega\tau), \tag{34}$$

which corresponds to a horizontal velocity of

$$v_\perp = a\Omega = \psi c_s(\Omega\tau). \tag{35}$$

The amplitude of the vertical shear, $\mathrm{d}v_R/\mathrm{d}z$, is then given by

$$S = \frac{\Omega a}{H} = \Omega^2\tau\psi. \tag{36}$$

If we add the assumption that the horizontal shear is damped by an *isotropic* viscosity with magnitude measured by the usual α, this, using equation (32), then implies that

$$a \sim \frac{\psi}{\alpha}H, \tag{37}$$

and the horizontal velocity is then given by[2]

$$v_\perp = \frac{\psi}{\alpha}c_s. \tag{38}$$

With this assumption the amplitude of the vertical shear, $S = \mathrm{d}v_R/\mathrm{d}z$, is given by

$$S = \frac{\Omega a}{H} = \frac{\psi}{\alpha}\Omega. \tag{39}$$

In order to relate the above description with the model described by equation (2), we note that in that equation the coefficient ν_2 acts formally on the radial derivative of the vertical component of the velocity (since it dissipates the warp). By the argument described above, the dissipation actually comes about because of damping of the resonantly induced, horizontal, shear motion that communicates the warp between different radii. The definition of ν_2 inherently implies that the rate at which energy is dissipated in the two processes must therefore be the same. Thus we must have

$$\nu_2\left\langle\frac{\mathrm{d}v_z}{\mathrm{d}R}\right\rangle^2 = \nu_z\left\langle\frac{\mathrm{d}v_R}{\mathrm{d}z}\right\rangle^2, \tag{40}$$

where angled brackets imply suitable vertical and azimuthal averages.

Now, in a warped disc $v_z = \psi R\Omega$ and $\mathrm{d}v_z/\mathrm{d}R = \psi\Omega$, which, in equation (40) gives

$$\nu_2 = \nu_z(\Omega\tau)^2 = \Omega H^2(\Omega\tau), \tag{41}$$

where, in the last equality, we have used the definition of ν_z, equation (31). This is equivalent to writing

$$\alpha_2 = \Omega\tau. \tag{42}$$

If the damping time-scale τ is indeed given by isotropic viscous dissipation, then, as above, we have $\tau\Omega = 1/\alpha$ and we finally recover the desired scaling of ν_2 with α in the linear case (cf. equation 5)

$$\frac{\nu_2}{\nu_1} \sim \frac{1}{\alpha^2}. \tag{43}$$

It is worth noting here that this result is somewhat counterintuitive, in that it implies that the damping of the warp occurs *more rapidly* when the viscosity is smaller! This comes about because a small value of isotropic viscosity (small α) permits a large resonant velocity ($v_R \propto 1/\alpha$). The dissipation rate depends on $\nu v_R^2 \propto 1/\alpha$, and so *increases* as α decreases. It is evident that the analysis must break down at some stage as $\alpha \to 0$.

[2] As an aside, we emphasize that this estimate is not valid for small values of α, because for $\alpha < \alpha_c$ the propagation becomes wave-like, and in that case $v_\perp \sim (\psi/\alpha_c)c_s$.

4.2 Comparison with the simulations

Most of the results shown in Fig. 8 come from a set of simulations all with $H/R = 0.013\,33$ and $\psi_{\max} = 0.026$ but with varying values of α. For these simulations we find that relationship between α and α_2 predicted by simple linear theory holds for values of α above around $\alpha \approx 0.16$ where $\alpha_2 \approx 3$. Below this critical value of α, α_2 remains approximately constant.

We now need to ask what mechanism(s) might give rise to such an effect, and in addition whether they correspond to some valid physics, or are merely numerical artefacts.

We have noted that from simple physical considerations we expect that $\alpha_2 \approx \Omega\tau$, where τ is the time-scale for damping the warp-induced horizontal shearing motions. Thus an upper limit to α_2 can come about through there being an upper limit to the damping time-scale τ; i.e. we need to identify a mechanism which prevents the damping taking place too slowly. For isotropic viscosity, the damping time-scale is such that $\Omega\tau = 1/\alpha$, so that the lower the viscosity, the longer the time-scale. Thus, paradoxically, in order to set an upper limit on α_2, i.e. in order to stop the warp being dissipated too fast, we need to find a mechanism which gives rise to *increased* dissipation. If there is such a process such that $\tau < K\Omega^{-1}$, where K is some constant, then we would find that $\alpha_2 < K = \alpha_{\max}$, in line with our findings.

So what physical or numerical process(es) might give rise to enhanced dissipation for small values of α?

We have noted that for isotropic viscosity the Mach number of the horizontal velocity induced by the warp is (to within factors of the order of unity)

$$\frac{v_\perp}{c_s} = \mathcal{M} = \frac{S}{\Omega} = \frac{\psi}{\alpha}. \tag{44}$$

The above equation shows that the horizontal resonant motion becomes supersonic for $\alpha \leqslant \psi$. In our simulations breakdown of the simple relation occurs for $\alpha \approx 0.16$ and $\psi \approx 0.026$, and therefore when $\mathcal{M} \approx 0.16$. Thus, breakdown occurs when the velocity difference across the disc thickness $|v_\perp(H) - v_\perp(-H)| \approx 0.32c_s$.

The radial shear flow induced by the warp can be clearly noted in Fig. 11, which displays the radial Mach number for simulation S6 at $t = 195$, at $R = 5$ and at different azimuthal positions, i.e. $\phi = 0$ (upper left-hand panel), $\phi = \pi/2$ (upper right-hand panel), $\phi = \pi$ (lower left-hand panel) and $\phi = 3\pi/2$ (lower right-hand panel) (here, we use a cylindrical coordinate system such that the z-axis lies along the local direction of the angular momentum vector $\boldsymbol{l}$). At height $z = \pm H$ the amplitude of this radial oscillation is $v_\perp/c_s \approx 0.1$, much less than the value of 0.37 expected for this simulation based on equation (44).

We have also run two simulations (S8 and S9) with a much larger warp amplitude, i.e. $\psi_{\max} = 1.3$. For simulation S9, we see that $\alpha \approx 0.1$, in which case we expect the Mach number of the radial resonant motion to be of the order of $\mathcal{M} \approx 13$, which is much larger than the Mach number $\mathcal{M} \approx 0.16$, above which we have observed the standard relation between α and α_2 to break down. This simulation should be compared with simulation S5, which has a very similar α and a very similar α_2, but a much smaller ψ and therefore a smaller predicted Mach number of $\mathcal{M} \approx 0.29$ (but still large enough to be in the saturated regime). We then see that increasing further the warp amplitude does not produce a significant decrease in α_2. Thus although for a larger warp the amount of dissipation increases, the dissipation time-scale appears to remain unchanged at $\tau \approx 3\Omega^{-1}$. In the case of simulation S8, instead, we have $\alpha \approx 0.26$, so that the predicted Mach number would be $\mathcal{M} \approx 5$. The corresponding low-amplitude simulation (S0), which has $\alpha \approx 0.28$ and predicted $\mathcal{M} \approx 0.1$, lies in the non-saturated regime, and in this case increasing the warp amplitude does result in an increased dissipation and a reduction in the value of α_2, which for S8 lies marginally below the predicted relation.

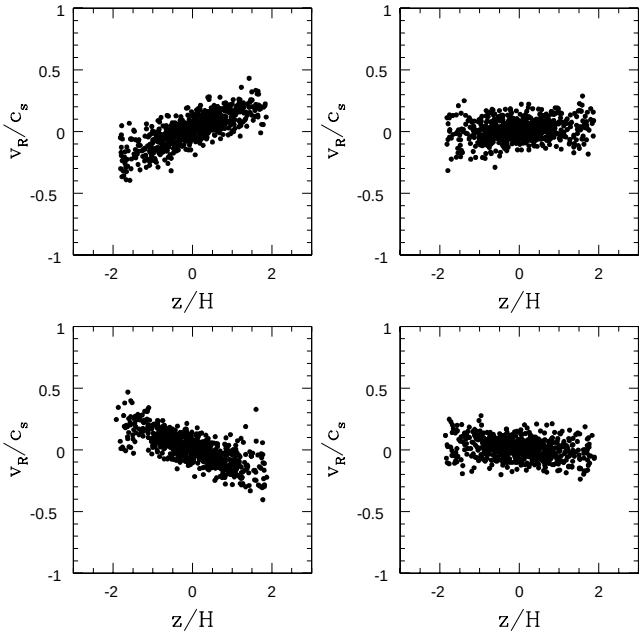

Figure 11. Run S6. The radial Mach number induced by the warp as a function of height above the disc at $R = 5$ and $\phi = 0$ (upper left-hand panel), $\phi = \pi/2$ (upper right-hand panel), $\phi = \pi$ (lower left-hand panel) and $\phi = 3\pi/2$ (lower right-hand panel). Here the cylindrical coordinate system is such that the z-axis lies along the local direction of the angular momentum vector $\boldsymbol{l}$. The disc scaleheight here is $H = 0.0665$. The amplitude of this flow at $z = \pm H$ is $\mathcal{M} \approx 0.1$.

4.3 High Mach number and enhanced dissipation

We have established that the results of our simulations can be understood if the internal disc flows, induced by the warp, result in higher dissipation than would be predicted by linear theory (assuming Navier–Stokes viscosity) when the Mach number of the flows exceeds a value of around $\mathcal{M} \sim 0.16$, i.e. when the relative flow velocity across a full disc thickness exceeds around $0.32c_s$. The internal flows predicted by the analytic theory are in fact of two types (see e.g. equations (102) and (103) of Ogilvie 1999). The first is the sinusoidally oscillating, linear shear flow discussed in Section 4 above,[3] which takes the form $v_R \propto z$ and oscillates with frequency Ω. This flow has an amplitude which scales linearly with ψ, and in the linear theory is indeed proportional to ψ/α. The second, whose magnitude depends more strongly on the size of the warp (i.e. it scales with ψ^2), is a sinusoidally pulsating, homologous flow, which is alternately expanding and contracting with angular frequency 2Ω and is of the form $v_z \propto z$. We have calculated the vertical gradients of these two types of flows by fitting a straight line to the velocity data, such as those shown in Fig. 11. We plot in Fig. 12 the results of this procedure as a function of azimuth for simulations S0b (left-hand panel) and S9 (right-hand panel). The typical uncertainty for these

[3] This radial (v_R) flow is part of a resonant epicyclic motion (see Section 4.1). It is therefore accompanied by an azimuthal flow of the form $v_\phi \propto z$, with amplitude $v_\phi = 2v_R$.

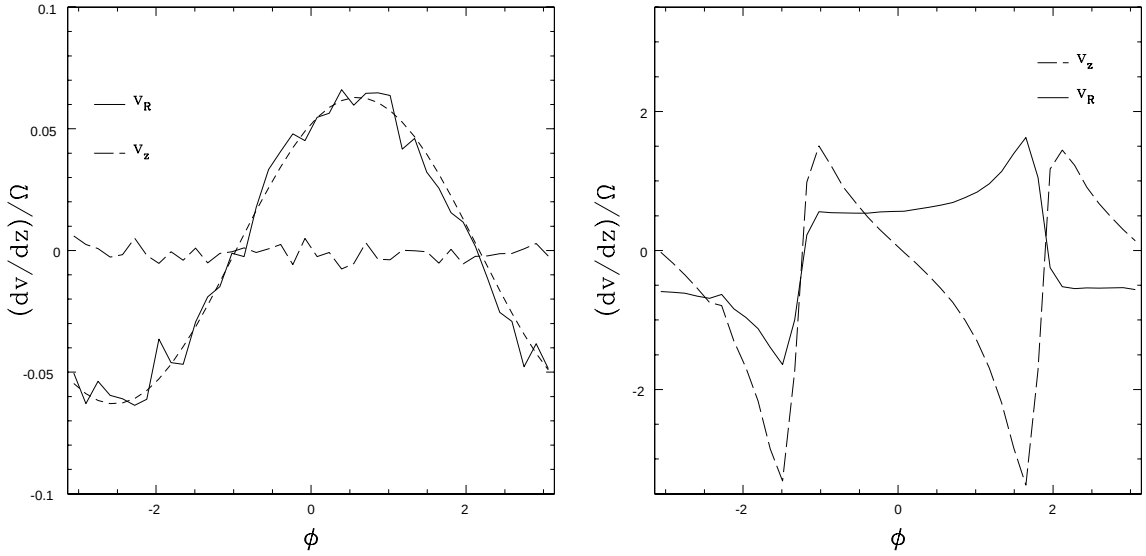

Figure 12. Vertical gradient of the resonant flow induced by the warp for simulations S0b, for which $\psi \approx 0.026$ (left-hand panel) and S9 (right-hand panel), for which $\psi \approx 1.3$. The linear theory predicts to first order in ψ that $\mathrm{d}v_\mathrm{R}/\mathrm{d}z \propto \psi \sin(\phi - \phi_0)$ and $\mathrm{d}v_z/\mathrm{d}z \propto \psi^2 \sin 2(\phi - \phi_0)$. The solid line shows $\mathrm{d}v_\mathrm{R}/\mathrm{d}z$, while the long-dashed line shows $\mathrm{d}v_z/\mathrm{d}z$. The short-dashed line is a sinusoidal fit to $\mathrm{d}v_\mathrm{R}/\mathrm{d}z$ for S0b. Here the cylindrical coordinate system is such that the z-axis lies along the local direction of the angular momentum vector $\boldsymbol{l}$.

data points ranges from 5 to 10 per cent. In both plots the solid line refers to the gradient of v_R, while the long-dashed line refers to the gradient of v_z. In the S0b case, the short-dashed line is a sinusoidal fit to the data points for v_R, with an amplitude equal to 0.063.

Let us first consider the case of simulation S0b. As discussed above, this simulation agrees well with the linear theory and with its prediction for the warp diffusion coefficient. In agreement with linear theory, for this low-amplitude warp, we find that the induced resonant flow is dominated by the radial component, the vertical one being negligible. The radial flow is indeed oscillating with frequency Ω as predicted by Ogilvie (1999). We have shown above (equation 39) that the amplitude of this oscillation should be (within factors of the order of unity) of the order of $\psi/\alpha \sim 0.093$ for S0b. Based on the results shown in Fig. 12 we can estimate the exact proportionality factor to be

$$\frac{\mathrm{d}v_\mathrm{R}}{\mathrm{d}z} \approx 0.65 \frac{\psi}{\alpha}\Omega. \tag{45}$$

We can now check the predicted scaling with ψ/α as we decrease the value of α. To this end, we have repeated the above analysis for S4 and S6, and we have found in both cases a roughly sinusoidal oscillation of $(\mathrm{d}v_\mathrm{R}/\mathrm{d}z)/\Omega$, with amplitude equal to $0.1 = 0.54\psi/\alpha$ for S4 and to $0.12 = 0.33\psi/\alpha$ for S6. Hence, we do not confirm the predicted scaling, the value of $\mathrm{d}v_\mathrm{R}/\mathrm{d}z$ for S6 being half of its predicted value. This is further evidence for enhanced dissipation. Note that this enhanced dissipation is only found for small values of α and it appears to increase as we increase the value of ψ/α.

The presence of both the radial and the vertical flow can be seen clearly in the right-hand panel of Fig. 12 and in Fig. 13 which corresponds to the run S9 which has a strong warp $\psi \sim 1$. The structure of this pulsating flow is shown in Fig. 14, where we show the Mach number in the z direction as a function of z at various azimuths in the disc (as before, the cylindrical coordinate system used here is such that the z-axis lies along the local direction of $\boldsymbol{l}$). As can be seen, the flow is highly supersonic, with disc elements approaching each other at velocities up to $\approx 10 c_\mathrm{s}$. As shown by Ogilvie (1999) these flows are formal solutions to the analytic equations, even for large

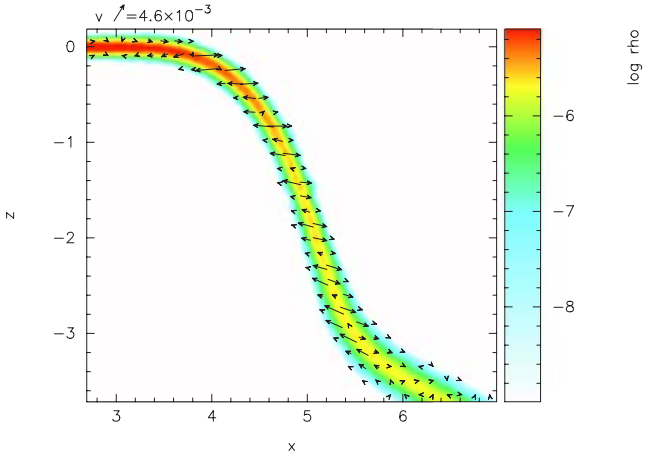

Figure 13. Colour plot of the vertical density structure of simulation S9, at $t = 185$, close to the warp location at $R = 5$. The arrows indicate the velocity structure. The vertically shearing radial flow induced by the warp has, in this large warp amplitude case, a significant component along the local vertical direction, determining a strong compression and rarefaction of the disc.

values of ψ, when the Mach numbers of the flows are expected to be large. Ogilvie (1999) does not, however, discuss the stability of such flows. Note that while both these flow appear to have the correct azimuthal periodicity (with frequency Ω for the radial component and 2Ω for the vertical one), they are not sinusoidal as additional Fourier components become important for large ψ (Ogilvie 1999, appendix). Note, in particular, the large amplitude and the sharp jumps of the vertical compression. Across a very narrow azimuthal range (and therefore over a time-scale much shorter than dynamical) the velocity changes by a factor much larger than the sound speed. Given the short time-scale, this change can be only due to pressure forces and artificial viscosity in this strongly compressional motion. Note also that the negative amplitude of the compressional motion is larger than the positive one, indicating that a large amount of

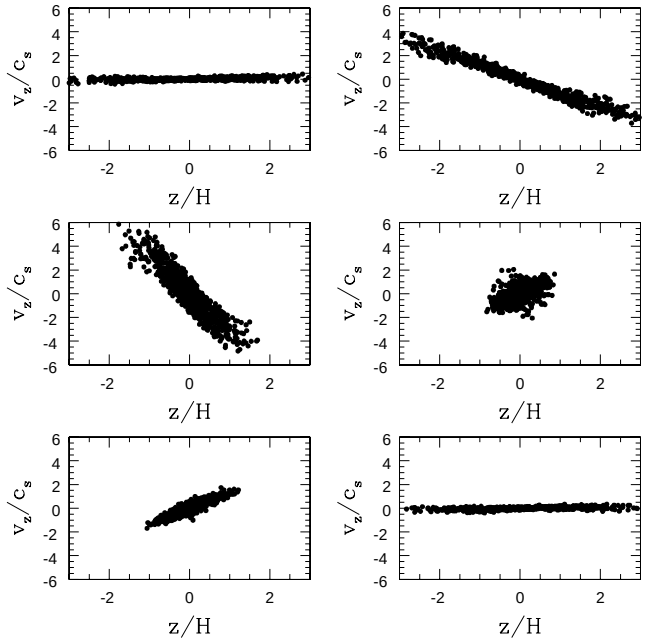

Figure 14. Velocity along the local direction of the angular momentum vector, in units of the local sound speed, for simulation S9, at $t = 185$, $R = 5$ and $\phi = 0$ (upper left-hand panel), $\phi = 0.3\pi$ (upper right-hand panel), $\phi = \pi/2$ (middle left-hand panel), $\phi = 0.6\pi$ (middle right-hand panel), $\phi = 0.7\pi$ (lower left-hand panel) and at $\phi = \pi$ (lower right-hand panel). Here, the coordinate system is such that the z-axis lies along the local direction of the angular momentum $\boldsymbol{l}$. Between $\phi = 0$ and $\pi/2$ the disc undergoes supersonic compression ($\mathrm{d}v_z/\mathrm{d}z < 0$), with a Mach number at $z = \pm H = \pm 0.0665$ approaching 3. Between $\phi = 0.5\pi$ and 0.6π these velocities are abruptly halted. At later phases the disc undergoes supersonic rarefaction ($\mathrm{d}v_z/\mathrm{d}z > 0$), until it reaches its original structure at $\phi = \pi$. The sequence is repeated between $\phi = \pi$ and 2π because the orbiting disc gas has to receive a vertical velocity nudge twice per orbit in order to prevent the orbits of gaseous disc elements from crossing.

kinetic energy is dissipated in the process. This also implies that the pulsating flow is not of the form $v_z \propto z$ at all times.

4.3.1 *A numerical explanation*

One possibility we need to address is whether the enhanced dissipation that we find in our simulations at high Mach number is a purely numerical effect. From the simulations presented here it is hard to be certain that it is not. But it is not easy to see what the effect might be.

It is certainly true that the flows are only moderately well resolved in our simulations: in order to treat discs which are thin enough that warp propagation occurs diffusively we were only able to consider simulations in which the average number of SPH smoothing lengths across the thickness of the disc is around 3.3. But the explanation cannot simply be due to lack of resolution, since our simulations agree with the analytic predictions for α_2 for the larger values of α, in the regime where the induced velocities are low, and analytic solutions are expected to be a good approximation. Disagreement only occurs once the Mach number of the induced shear flow increases to about 0.16 across a scaleheight H, or to about 0.096 across a smoothing length h. In addition we obtain similar results for α_2 whether the SPH viscous switch is turned on or off. Thus it seems to us unlikely that either lack of resolution or the nature of the SPH stress tensor is the cause of the disagreement.

It is evident, however, that the disagreement between the approximate analytic theory and the numerical simulations in respect of precession rates does depend on the nature of the numerical viscosity. Our finding that none of our simulations confirms the analytic predictions, and that even for the same formal α we obtain opposite signs for the precession rates depending on whether or not the viscous switch is on or off, implies that the induced precession is very sensitive to the precise details of disc viscosity. This implies that if the viscous stress tensor within the disc is not precisely of the Navier–Stokes form, and as we have remarked above it is very unlikely that it is, then the analytic predictions for the precession rates are unlikely to be relevant to real accretion discs. Luckily, as we have remarked above, such precession is in general only a minor effect.

4.3.2 *A physical explanation*

When the Mach numbers of the internally induced flows approach unity it seems physically plausible that such flows might become unstable. If such instabilities gave rise to enhanced dissipation, then they could provide an explanation for our results.

Instabilities in a steady shear flow typically grow at a rate $\gamma \sim S$, the rate of shear (e.g. Drazin & Reid 1981). In an oscillating shear flow one might expect instability to be suppressed unless the growth rate exceeds the rate of oscillation, i.e. unless $S > \Omega$. However, Gammie et al. (2000) demonstrate that shear instabilities, caused by parametrically unstable modes, can exist with $\gamma \sim S$ even when $S < \Omega$ (and in particular they predict instability for $S/\Omega \sim \mathcal{M} > 30\alpha$). For the largest scale modes of size $\sim H$ the damping time-scale would be $\sim H^2/\nu \sim \tau \sim (\alpha\Omega)^{-1}$. Thus we might expect shear instabilities to be able to grow when $\gamma\tau > 1$, i.e. when $\psi > \alpha^2$ or when $\mathcal{M} > \alpha$. Using these arguments, for the set of simulations with $\psi = 0.026$, we would then expect shear instabilities to occur when $\alpha < 0.16$, which is in agreement with our findings. To discover whether this agreement is fortuitous or not will require further work.

We have not demonstrated, however, that a shear flow becomes unstable simply because it is supersonic, and to this extent the arguments we put forward here are speculative. Indeed one could argue in this case that the particles on the top and bottom of the disc are essentially following free, elliptical trajectories around a central point mass. However, this is not strictly true because fluid elements separated vertically by $\sim H$ do need to interact, and to receive a vertical velocity nudge of order $\sim c_s$ twice per orbit, i.e. on a time-scale $\sim(1/2)\Omega^{-1}$, in order to remain a distance $\sim H$ apart. Once the horizontal fluid motions become supersonic, i.e. once $S \sim \Omega$, the fluid elements separated vertically by $\sim H$ can no longer maintain pressure communication. Then unless the flow adheres exactly to the simple solution found in analytic theory, without any perturbations, then the required velocity nudge has to be communicated through shocks.

Indeed it is this vertical velocity nudge, required twice per orbit, which gives rise to the compressive, pulsatory flow of the form $v_z \propto z$ with frequency 2Ω. Again for this motion, unless the flow adheres exactly to the analaytical solution, and there are no perturbations present within the disc, then once the pulsatory motions approach sonic velocities, the pulsations must result in shock formation and enhanced dissipation.

5 CONCLUSIONS

Using numerical simulations we have explored the propagation and damping of warped accretion discs in the regime ($\alpha \geqslant \alpha_c$) when propagation occurs diffusively. In this regime we find that warp propagation is described reasonably well by the simple equation given by Pringle (1992), which involves just two viscosity parameters α and α_2. This is true, and gives the same α_2–α relationship, whether or not the SPH 'viscous switch' is turned on. As expected from linear analysis, and from the simple physical arguments presented in Section 4, we find that as α decreases, α_2 increases and at large values of α our simulations agree with the predictions of previous analytic work. This is the first time that this has been demonstrated numerically. We also find, however, that, if α decreases below some value $\alpha_{\rm sat} \approx 0.16$, enhanced dissipation occurs which acts to damp the warp-driven, internal, resonant motions, and so prevents a further rise in α_2. We find a maximum value of $\alpha_2 = \alpha_{\rm max} \approx 3$–4. We speculate that this maximum value comes about because at low values of α the induced horizontal shearing motions become close to sonic, and are therefore subject to instabilities and enhanced dissipation. Further numerical work is required to test these ideas.

In line with the expectations of linear theory we also find that the warp induces precession which causes the disc to twist. As predicted, the precession time-scales are typically longer than the time-scales for warp propagation and damping. However, the exact values of the precession rates, and even the direction of precession, are not in agreement with the predictions of linear theory. This presumably reflects at some level the degree to which SPH viscosity fails to provide an accurate model of isotropic Navier–Stokes viscosity, which is assumed in the linear calculations. Indeed it is for the simulations with the 'viscous switch' turned on (so that dissipation only occurs in regions of converging flow), for which the SPH viscosity can be expected to be least like Navier–Stokes, that the direction of precession is the opposite to that predicted by linear theory. Since the viscosity in real accretion discs is unlikely to be Navier–Stokes, this implies that theoretical predictions of warp-induced precession rates need to be treated with caution.

The numerical method we have used is SPH. This has the advantage of being a Lagrangian code, and so can deal straightforwardly with thin warped discs, without the need of careful treatment of strong density contrasts across neighbouring grid cells. It has, however, the disadvantage that the fluid viscosity (α) depends on particle density, which therefore implies that varying viscosity involves varying numerical resolution. As can be seen from Table 1, even using one or two million particles, for the parameter ranges we are able to investigate the number of smoothing lengths per disc scaleheight is never very large, varying from around 10 for the thickest disc down to 1.7 for the thinnest disc. It is further worth noting that although we do find evidence of enhanced dissipation as α decreases, i.e. as the amplitude of the internal resonant shearing motions increases, it is not clear that at this resolution the fluid dynamical effects which give rise to such enhanced dissipation (e.g. fluid instabilities, shocks, etc.) are being captured correctly. Thus the values we find for $\alpha_{\rm max}$ need to be treated with appropriate caution. In addition we find that the small precessional effects induced by the warp depend sensitively on the exact implementation of the SPH viscosity. It would be instructive to compare the results we obtain here with results obtained using a grid-based numerical technique which would be better able to deal with shock capturing, and thus better able to identify the source of the enhanced dissipation we find at large amplitudes of the horizontal shear motion. It is also important to incorporate magnetic effects, since it is these which are thought to be the basic cause of disc 'viscosity', and it seems likely that these may not be well modelled by the assumption of an isotropic Navier–Stokes viscosity.

ACKNOWLEDGMENTS

We thank Gordon Ogilvie for useful advice which led to a redrafting of an earlier version of this paper, the anonymous referee for a constructive report and Steve Lubow for interesting discussions. The simulations described in this paper have been performed at the UK Astrophysical Fluid Facility (UKAFF). The visualization of the simulations shown in Fig. 13 has been made using the SPLASH software by Dan Price.

REFERENCES

Artymowicz P., Lubow S. H., 1994, ApJ, 421, 651
Balbus S. A., Hawley J. F., 1998, Rev. Mod. Phys., 70, 1
Bardeen J. M., Petterson J. A., 1975, ApJ, 195, L65
Bate M. R., Bonnell I. A., Price N. M., 1995, MNRAS, 277, 362
Begelman M. C., King A. R., Pringle J. E., 2006, MNRAS, 370, 399
Benz W., 1990, in Buchler J., ed., The Numerical Modelling of Nonlinear Stellar Pulsations. Kluwer, Dordrecht
Chiang E. I., Murray-Clay R. A., 2004, ApJ, 607, 913
Coleman C. S., Dopita M. A., 1992, Proc. Astron. Soc. Aust., 10, 107
Drazin P. G., Reid W. H., 1981, NASA STI/Recon Technical Report A, 82, 17950
Fromang S., Papaloizou J., 2007, A&A, 468, 1
Gammie C. F., Goodman J., Ogilvie G. I., 2000, MNRAS, 318, 1005
Gingold R. A., Monaghan J. J., 1977, MNRAS, 181, 375
Herrnstein J. R., Greenhill L. J., Moran J. M., 1996, ApJ, 468, L17
King A. R., Pringle J. E., 2006, MNRAS, 373, L90
King A. R., Pringle J. E., Livio M., 2007, MNRAS, 376, 1740
Larwood J. D., Nelson R. P., Papaloizou J. C. B., Terquem C., 1996, MNRAS, 282, 597
Lodato G., Pringle J. E., 2006, MNRAS, 368, 1196
Lubow S. H., Ogilvie G. I., 2000, ApJ, 538, 326
Lubow S. H., Ogilvie G. I., Pringle J. E., 2002, MNRAS, 337, 706
Lucy L. B., 1977, AJ, 82, 1013
Monaghan J. J., 1992, ARA&A, 30, 543
Murray J. R., 1996, MNRAS, 279, 402
Nelson R. P., Papaloizou J. C. B., 1999, MNRAS, 309, 929
Nelson R. P., Papaloizou J. C. B., 2000, MNRAS, 315, 570
Ogilvie G. I., 1999, MNRAS, 304, 557
Ogilvie G. I., 2000, MNRAS, 317, 607
Ogilvie G. I., Dubus G., 2001, MNRAS, 320, 485
Papaloizou J. C. B., Lin D. N. C., 1995, ApJ, 438, 841
Papaloizou J. C. B., Pringle J. E., 1983, MNRAS, 202, 1181
Papaloizou J. C. B., Terquem C., Lin D. N. C., 1998, ApJ, 497, 212
Pessah M. E., Chan C. K., Psaltis D., 2007, preprint (astro-ph/0705.0352)
Pringle J. E., 1992, MNRAS, 258, 811
Pringle J. E., 1996, MNRAS, 281, 357
Scheuer P. A. G., Feiler R., 1996, MNRAS, 282, 291
Shakura N. J., Sunyaev R. A., 1973, A&A, 24, 337
Torkelsson U., Ogilvie G. I., Brandenburg A., Pringle J. E., Nordlund Å., Stein R. F., 2000, MNRAS, 318, 47
Wijers R. A. M. J., Pringle J. E., 1999, MNRAS, 308, 207

This paper has been typeset from a TEX/LATEX file prepared by the author.